2 P

BEADING AND SPIKING PHENOMENA IN THE M551 METALS MELTING EXPERIMENT

ADDENDUM TO FINAL REPORT

By

C. Fan
M. R. Brashears

1 May 1974

Prepared under Contract No. NAS8-28729

Lockheed Missiles & Space Company, Inc.
Huntsville Research & Engineering Center
Huntsville, Alabama

AUG 19..
RECEIVED
NASA STI FACILITY
INPUT BRANCH

For

NASA-GEORGE C. MARSHALL SPACE FLIGHT CENTER

(NASA-CR-120352) BEADING AND SPIKING PHENOMENA IN THE M551 METALS MELTING EXPERIMENT Addendum to Final Report (Lockheed Missiles and Space Co.) 36 p HC $5.00
N74-30991
Unclas
CSCL 11F G3/17 16712

FOREWORD

This report summarizes the results of some additional studies regarding the beading and spiking phenomena observed in the M551 Metals Melting experiment conducted in the M512 Materials Processing Facility aboard the Skylab Laboratory. This effort was performed by personnel in the Fluid Mechanic Applications Group of the Lockheed-Huntsville Research & Engineering Center for the NASA-Marshall Space Flight Center.

This work was performed under the direction of Mr. R. M. Poorman, S&E-ASTN-MM, who was the principal investigator on the M551 space experiment.

PRECEDING PAGE BLANK NOT FILMED

BEADING AND SPIKING PHENOMENA IN THE M551 METALS MELTING EXPERIMENT

ADDENDUM TO FINAL REPORT

By

C. Fan

and

M. R. Brashears

Lockheed Missiles & Space Company, Inc.
Huntsville, Alabama

ABSTRACT

A study was made regarding the beading and spiking phenomena observed in the M551 Metals Melting experiment conducted during the Skylab I mission in June 1973. An analysis was made of the beading phenomenon based on the Kármán vortex shedding theory. The results tend to support the hypothesis that beading which occurred in the stainless steel and tantalum samples was a Kármán vortex street formation.

A dynamic model of cavity oscillation is discussed to explain the spiking phenomenon which was observed in the stainless steel and tantalum samples. Calculations of spiking frequency indicate that the intensity of spiking depends primarily on the vapor pressure and surface tension properties of the material, and is only slightly affected by the level of gravitational acceleration.

PRECEDING PAGE BLANK NOT FILMED

CONTENTS

LIST OF TABLES

LIST OF ILLUSTRATIONS

PRECEDING PAGE BLANK NOT FILMED

LIST OF ILLUSTRATIONS (Concluded)

SECTION I. INTRODUCTION

The M551 Metals Melting experiment was one of the spaceflight experiments conducted in the M512 Materials Processing Facility during the Skylab I mission in June 1973. The M512 Facility was an experimental apparatus designed and developed by NASA for conducting materials processing experiments in space. The facility consisted of a spherical processing chamber approximately 40 cm in diameter. The energy source in the M512 unit was an electron beam with a power capacity of between 1.0 and 1.6 kilowatts. A vacuum environment could be created by venting the chamber directly to outer space. During the Skylab I mission, Astronaut Charles Conrad performed the following experiments in the M512 facility: (1) the M551 Metals Melting experiment; (2) the M552 Exothermic Brazing experiment; (3) the M553 Sphere Forming experiment; (4) the M479 Zero-Gravity Flammability experiment; (5) the M554 Composite Casting experiment; and (6) the M555 Gallium Arsenide Crystal Growth experiment.

Lockheed was responsible for performing studies to analyze the results of the M551, M552 and M553 experiments, including conducting ground-based (1-g) tests and KC-135 (low-g) aircraft flight tests. The results of these studies and some other directly related investigations have been documented [1 through 23].

The present document reports the results of some additional studies regarding the bending and spiking phenomena observed in the M551 Metals Melting experiment as well as in some ground-based electron beam welding experiments. The M551 experiment consisted of a rotating metal disk mounted perpendicular to the electron beam (eb) heat source with the eb impingement point located 6 cm from the center of rotation. The velocity of the beam relative to the impingement point was 1.61 cm/sec with a corresponding radial acceleration of 5.09×10^{-4} g. The eb was focused to approximately 0.15 cm diameter with a beam power of 1.6 kW. The three materials used in the experiment were 2219 aluminum, 321 stainless steel and tantalum. The thickness of the materials varied with angular position around the disk. During the continuous weld portion of each disk, both full and partial penetration of the disk was achieved by using a constant power input but a varying disk thickness. For eack disk, the continuous weld was followed by a dwell portion. In the dwell portion of the weld, the disk was stationary while the electron beam impinged on the thick segment of the disk, thus creating a large molten pool. The electron beam was then shut off and the pool allowed to solidify [22].

SECTION II. BEADING PHENOMENON

The M551 Metals Melting experiment was conducted by Astronaut Charles Conrad during the Skylab I mission in June 1973. During the experiment, motion pictures were taken for each of the three metal disks. The motion pictures taken along with the experiment specimens were then brought back to earth for analysis. Shown in Figures 1, 2 and 3 are three photographs taken of the 321 stainless steel, 2219 aluminum and tantalum specimens after being subjected to electron beam impingement in the M551 flight experiment. For comparison purposes, ground-based tests were also made of the same specimens under similar operating conditions. The photographs taken for the three M551 materials during ground tests are shown in Figures 4, 5 and 6. The most striking phenomenon appearing in these photographs is the "beading" effect which occurs simultaneously with total eb penetration in the stainless steel and tantalum specimens. No beading is exhibited in the aluminum sample, however.

It was hypothesized [20 and 22] that the forming of beads after the passage of an electron beam was related to the vortex shedding phenomenon. When a cylinder moves through a fluid above a certain speed, the cylinder sheds behind its wake a periodic pattern of vortices which move alternatively clockwise and counterclockwise. This vortex formation is known as Kármán vortex street. A sketch showing the streamlines of a Kármán vortex street is given in the sketch below.

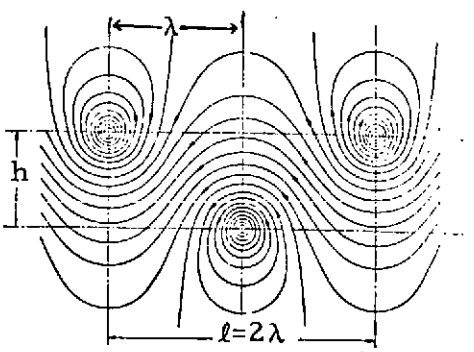

Kármán Vortex Street (Diagrammatic); Stream-lines Drawn in a System of Coordinates Moving with the Vortex Street

In this sketch, λ is the wave length or vortex spacing and h is the separation distance between the two rows of vortices.

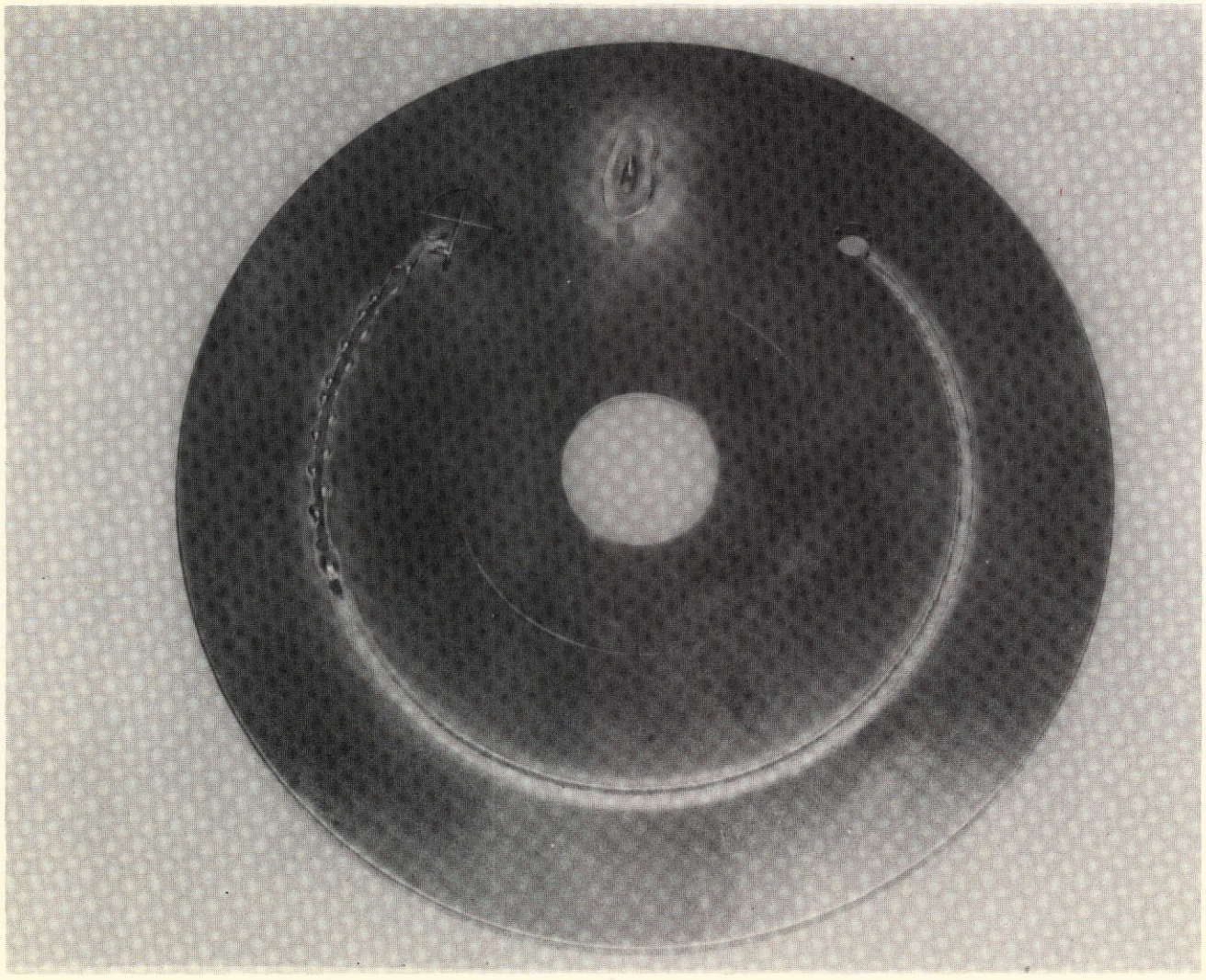

FIGURE 1. STAINLESS STEEL DISK AFTER M551 FLIGHT TESTS

PRECEDING PAGE BLANK NOT FILMED

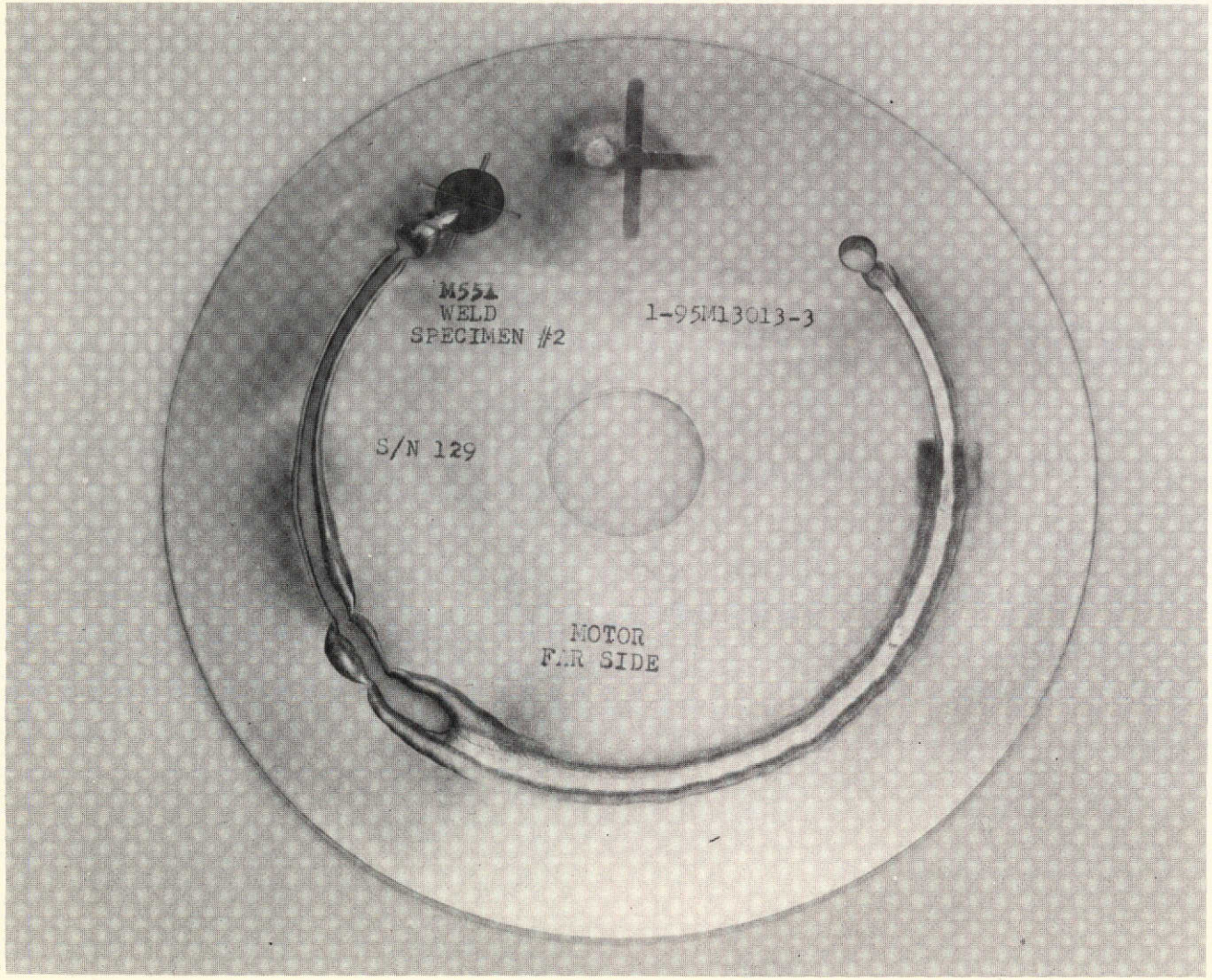

FIGURE 2. ALUMINUM DISK AFTER M551 FLIGHT TESTS

PRECEDING PAGE BLANK NOT FILMED

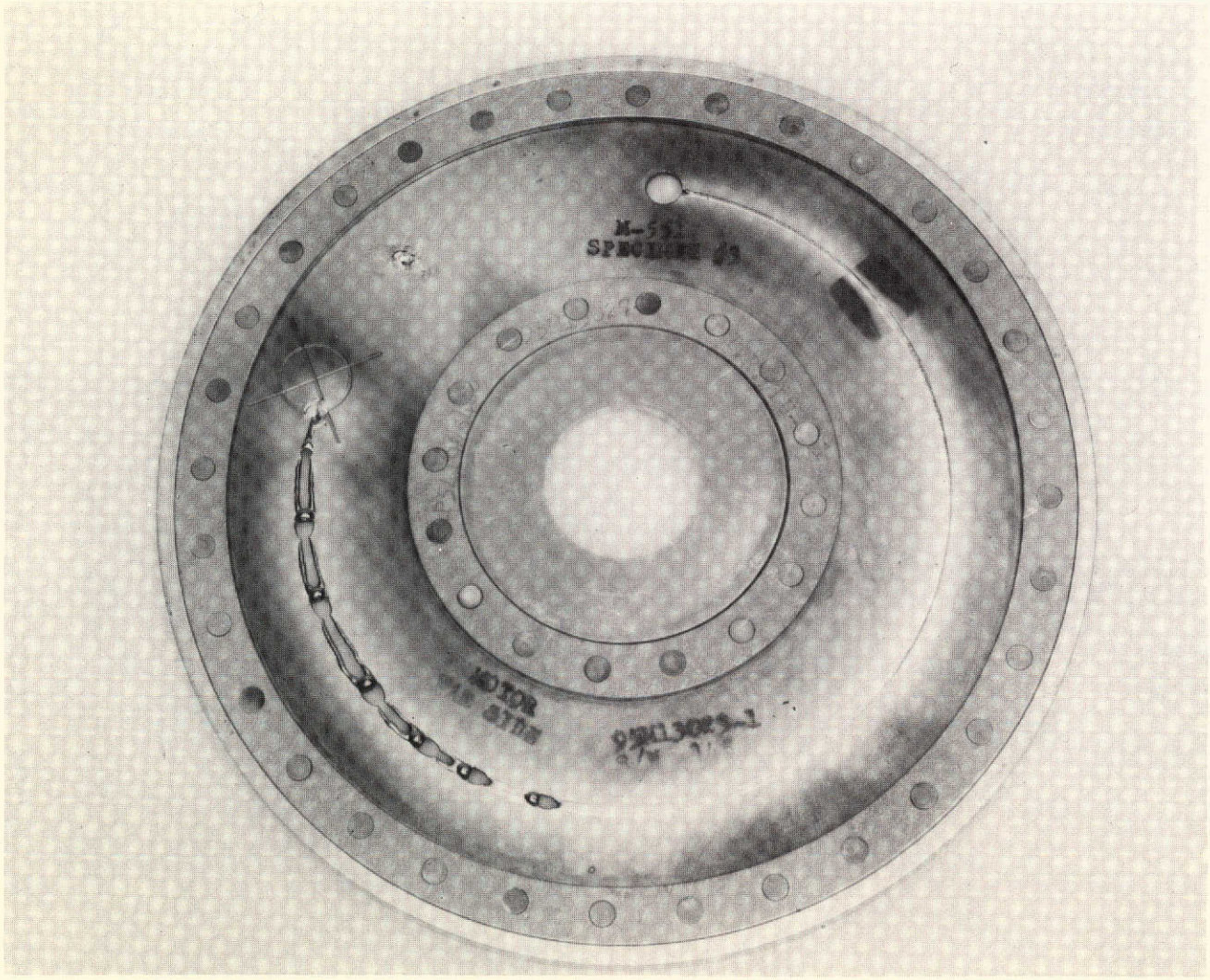

FIGURE 3. TANTALUM DISK AFTER M551 FLIGHT TESTS

PRECEDING PAGE BLANK NOT FILMED

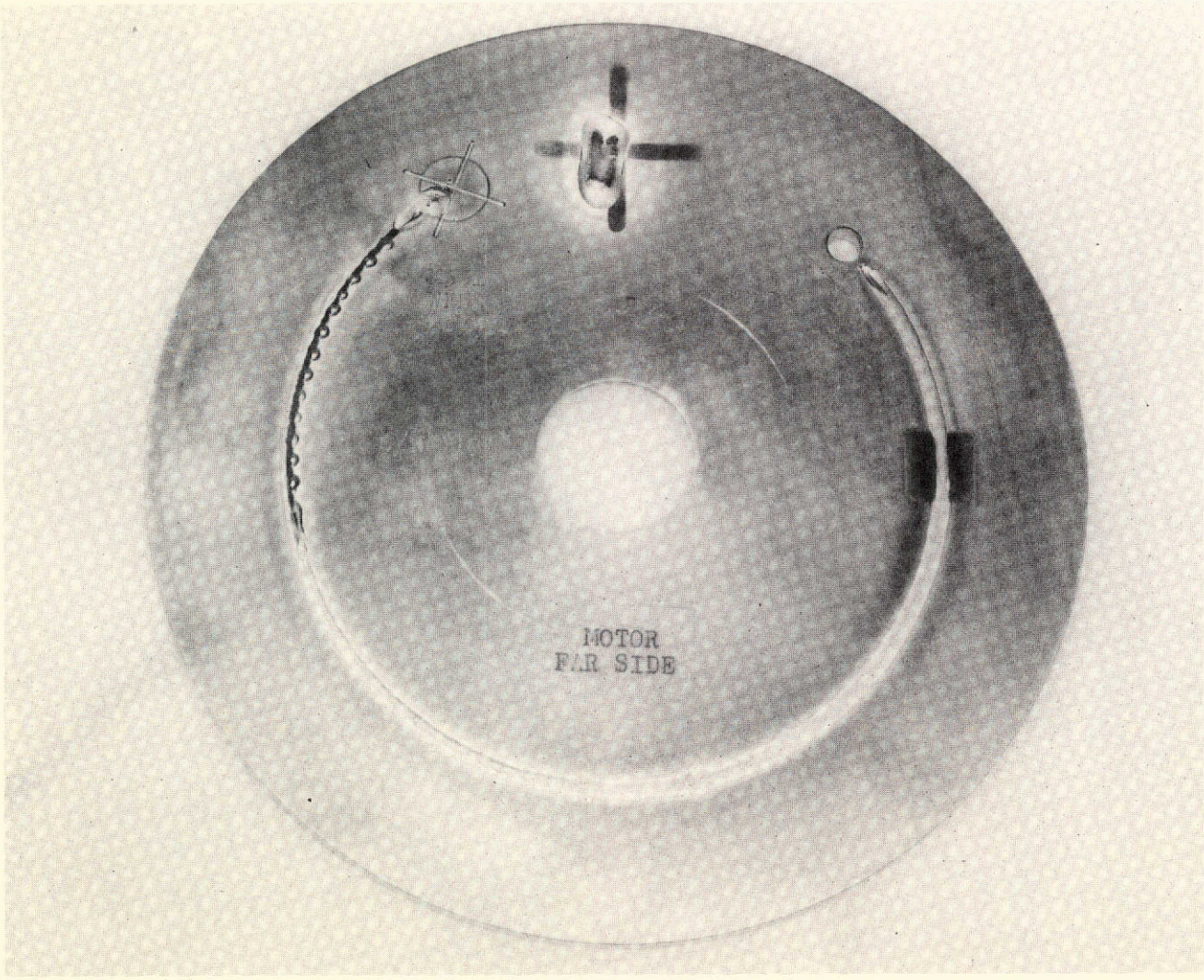

FIGURE 4. STAINLESS STEEL DISK AFTER M551 GROUND-BASED TESTS

PRECEDING PAGE BLANK NOT FILMED

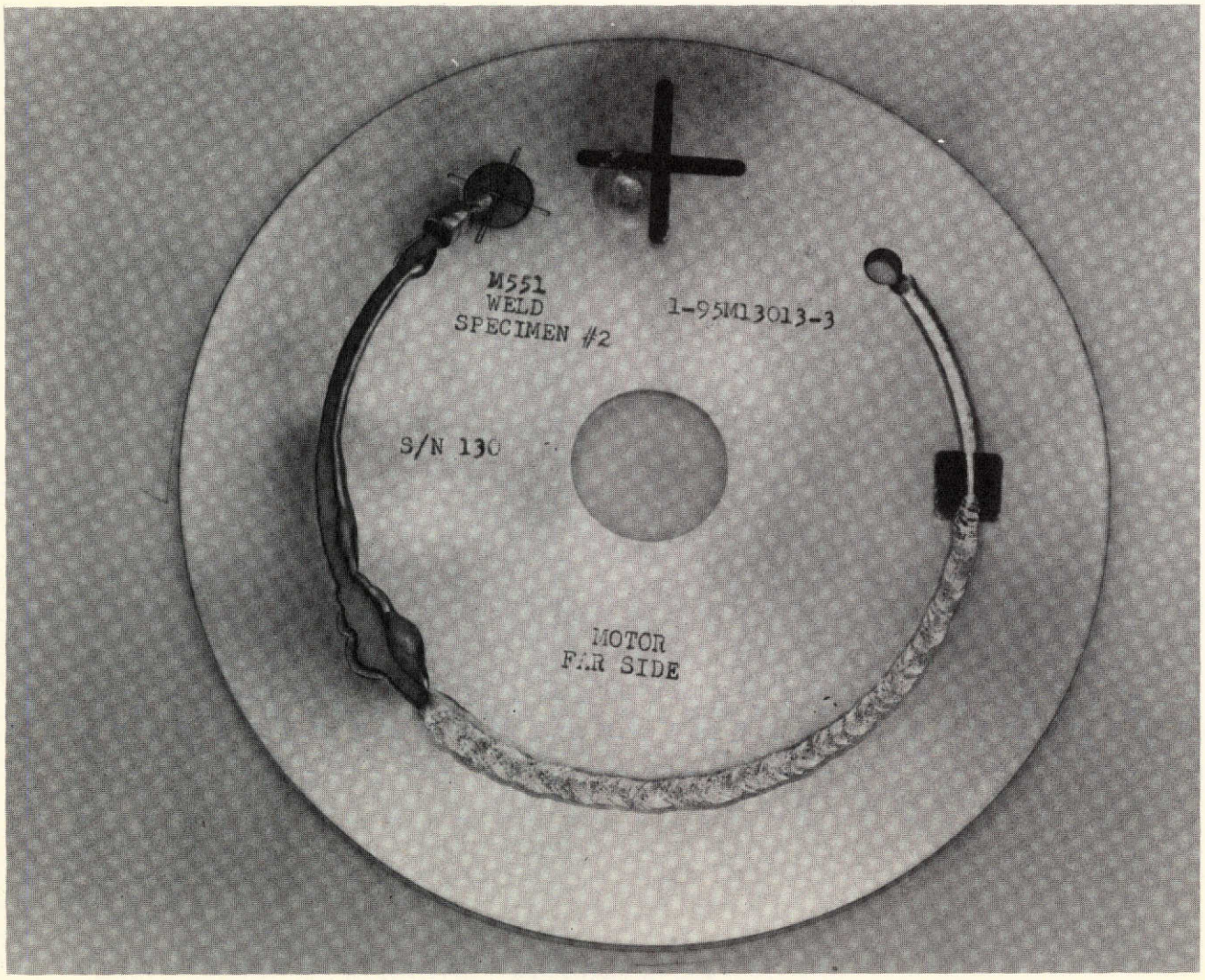

FIGURE 5. ALUMINUM DISK AFTER M551 GROUND-BASED TESTS

PRECEDING PAGE BLANK NOT FILMED

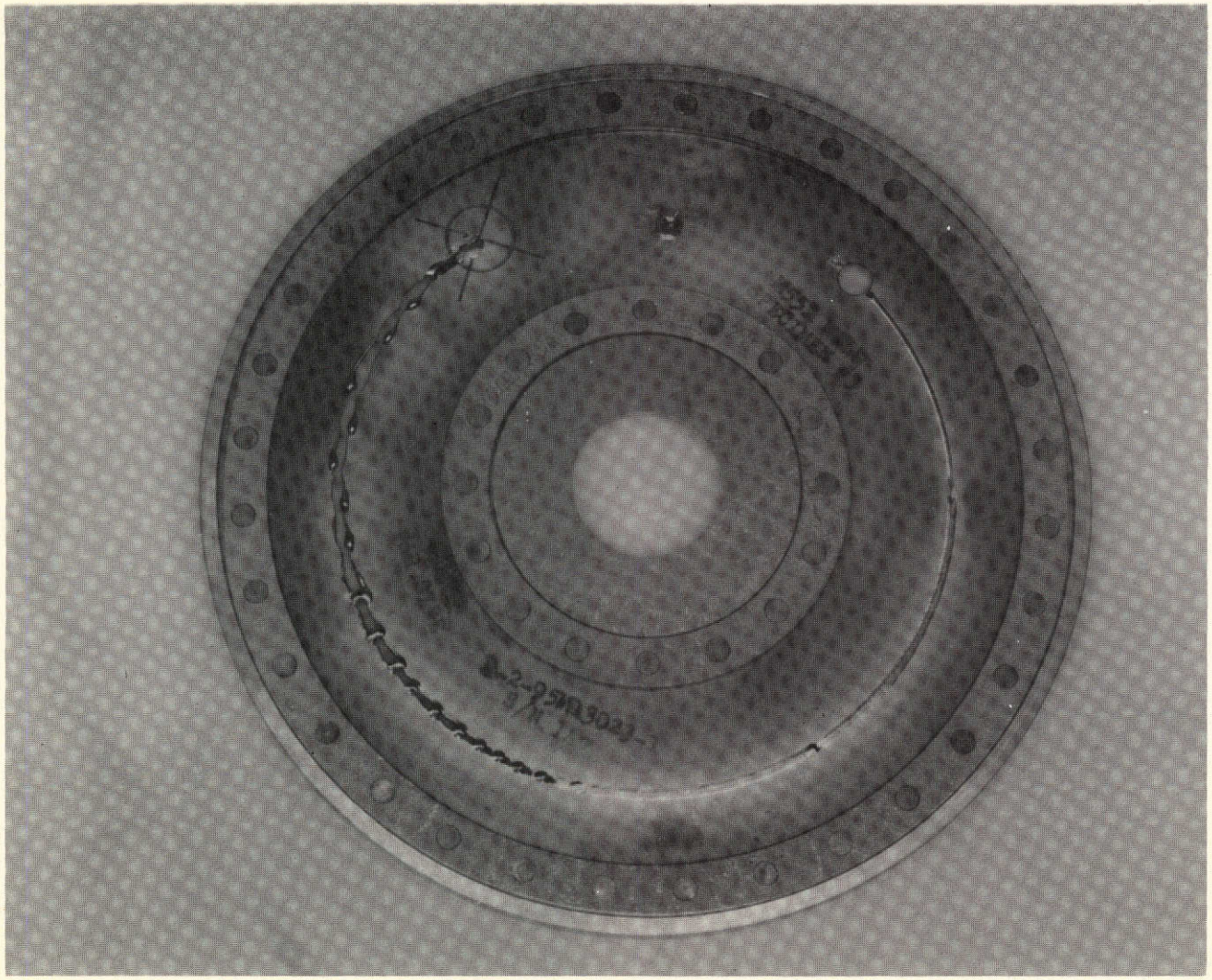

FIGURE 6. TANTALUM DISK AFTER M551 GROUND-BASED TESTS

The shedding frequency, f, i.e., the number of vortices shed per unit time, is dependent upon the density, ρ, and viscosity, μ, of the fluid, the diameter of the cylinder, D, and the velocity, V, with which the cylinder moves relative to the fluid. The interrelationship between these quantities can be correlated in terms of two dimensionless parameters known as Strouhal number, S, and Reynolds number, R, which are defined as

$$S = \frac{f \times D}{V}$$

$$R = \frac{\rho V D}{\mu} .$$

The relationship between S and R was obtained experimentally by Roshko [24] for a fluid in large extent. Roshko's experimental results and empirical equations between S and R are shown in Figure 7.

The wave length of the vortices, λ, is given by

$$\lambda = \frac{V - v}{f} \qquad (1)$$

where v is the velocity of the vortex which decreases with the distance from the cylinder. The magnitude of v is only of the order of 4 to 5% at a distance of 10 to 20 diameters downstream of the cylinder. The value of v is even smaller when the flow is confined by side walls. For all practical purposes v can be neglected in Eq. (1).

With the above basic background information, one can compile a list of data regarding the M551 space flight and ground-based experiments in view of the vortex shedding hypothesis. The compiled data are tabulated in Table 1. The manner in which these data are obtained is described as follows.

The two temperatures selected for calculation for each of the three M551 specimens correspond to the melting temperature and predicted maximum temperature [20]. The Reynolds number was calculated based on the velocity of the electron beam relative to the disk, the focusing diameter of the electron beam, and the density and viscosity of the molten metal. The viscosity of liquid metals depends strongly on temperature. The following equation was used in computing the viscosity of the molten metals

$$\mu = \mu_o e^{E/\Re T} \qquad (2)$$

PRECEDING PAGE BLANK NOT FILMED

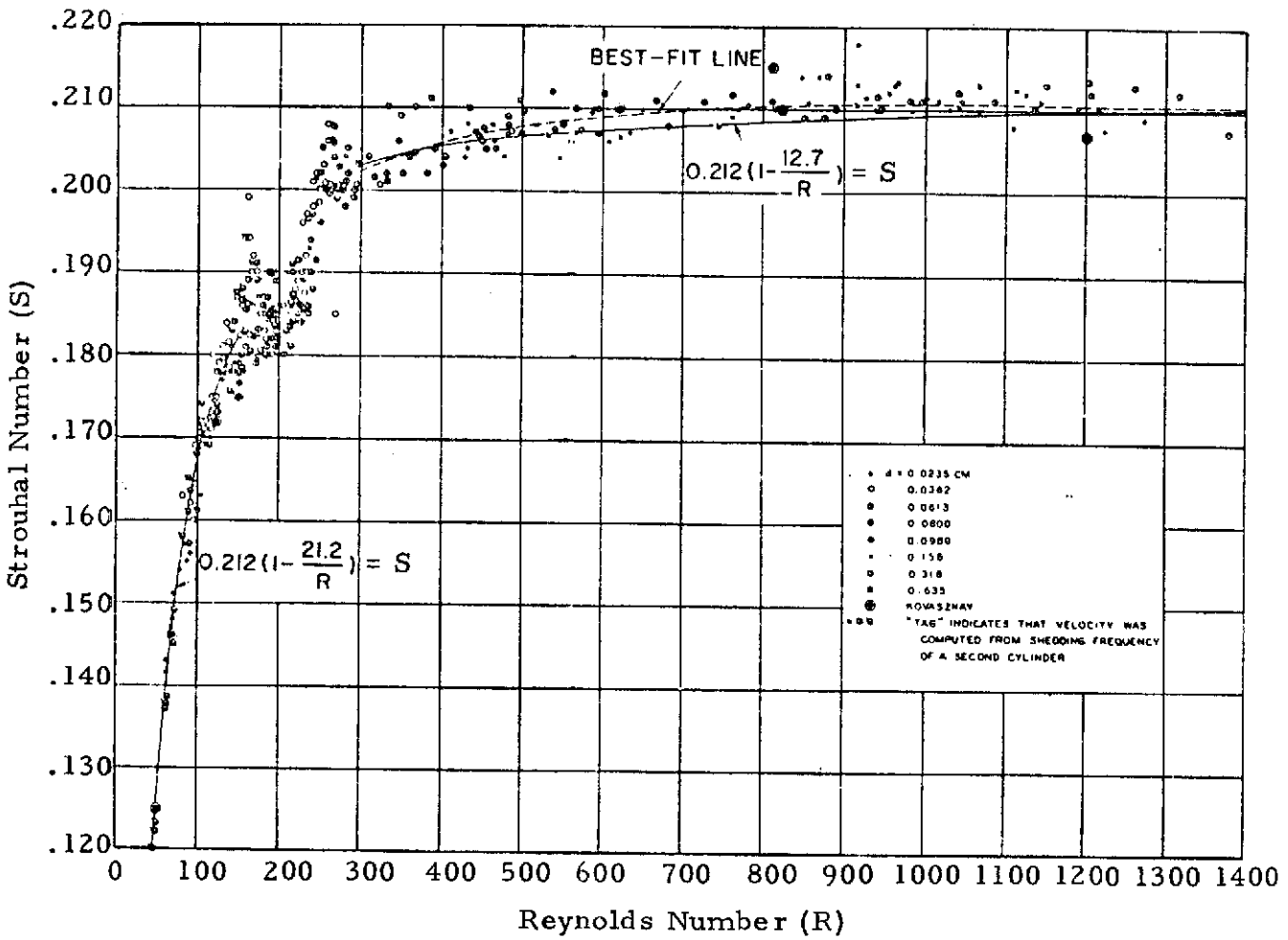

FIGURE 7. STROUHAL NUMBER AS FUNCTION OF THE REYNOLDS NUMBER FOR VORTEX SHEDDING BEHIND A CYLINDER [24]

Table 1

COMPARISON OF THEORETICAL AND EXPERIMENTAL BEAD SPACING

M551 Materials	Temperature T (^{o}K)	Reynolds Number R	Strouhal Number S	Shedding Frequency f (Hz)	Theoretical Bead Spacing λ (cm)	Flight Bead Spacing λ (cm)	Ground Bead Spacing λ (cm)
321 Stainless Steel	1700	35	—	—	—	0.356	0.418
	2253	72.5	0.15	1.61	1.0		
2219 Aluminum	916	50	—	—	—	—	—
	2113	171	0.185	1.98	0.81		
Tantalum	3270	121	0.175	1.88	0.86	1.57	0.94
	3833	181	0.188	2.02	0.80		

where μ_o is a reference viscosity, E is the activation energy, $\Re$ is the universal gas constant, and T is the absolute temperature. The values of μ_o and E are different for different materials. For example, for the stainless steel specimen, μ_o and E_o are estimated to be [25]

$\mu_o = 0.37$ Centipoise

$E = 9.9$ Kcal/gm-mole-^oK

After the Reynolds number was calculated, the Strouhal number was derived from Figure 7. The shedding frequency can then be computed from the definition of the Strouhal number. The theoretical bead spacing (i.e., wave length) is calculated from Eq. (1) by neglecting v. The data listed in the last two columns of Table 1 are the average bead spacings obtained by direct measurements from Figures 1 through 6.

It is seen in Table 1 that except for the aluminum specimen for which no beads were observed, the predicted bead spacing based on the vortex shedding theory and the experimentally measured average bead spacing are in good qualitative agreement. Quantitative agreement was not expected since the geometry and boundary conditions of the M551 Metals Melting experiment were not quite the same as those for a long solid cylinder moving in a fluid of large extent.

The theoretically predicted shedding frequency for each of the three specimens is also compared in Table 2 with corresponding experimental results for both space flight and ground-based tests. Again, good qualitative agreement among the data is obtained, except for the aluminum specimen.

It is theorized that surface tension must play an important role in the formation of beads from the vortices of the liquid metal during cooling and solidification. The larger the surface tension, the more easily the beads can be formed. The magnitude of surface tension (σ) for the three M551 materials at their respective melting temperatures are as follows:

321 stainless steel,	σ = 1750 dyne/cm
2219 aluminum,	σ = 737 dyne/cm
Tantalum,	σ = 2150 dyne/cm

It is noted that the surface tension of 2219 aluminum is only 30 to 40% of that of the other two materials. Thus, it is quite possible that during the flight and ground tests with the 2219 aluminum specimen, vortices were present but no beads were formed due to insufficient surface tension force.

Table 2

COMPARISON OF THEORETICAL AND EXPERIMENTAL SHEDDING FREQUENCY

M551 Material	Theoretical Shedding Frequency (Hz)	Flight Shedding Frequency (Hz)	Ground Shedding Frequency (Hz)
321 Stainless Steel	1.61	4.52	3.85
2219 Aluminum	1.98	—	—
Tantalum	2.02	1.03	1.71

The above analysis is, of course, qualitative. The motion of the molten metal in the wake of an electron beam is influenced by many factors. In addition to the parameters involved in the definitions of Strouhal and Reynolds numbers, the state of the fluid motion is influenced by the thickness of the disk, confining side walls (between molten and solid metals), free surface and surface tension effects, as well as non-uniform temperature distributions.

In general, the effect of confining side walls is to increase the critical Reynolds number for the onset of vortex shedding. According to Taneda [26], when the ratio of the diameter of the cylinder to the distance between the walls is increased from 0 to 0.5*, the critical Reynolds number is increased from 45 to about 80. Shair et al. [27] have also conducted experiments showing the effect of confining walls on the stability of the wake behind a circular cylinder. Their results indicated a more pronounced effect than that reported by Taneda. This may also explain the absence of beading in the aluminum specimen, since the calculated minimum Reynolds number for this case is only about 50. It appears, however, that confining wall effects alone do not explain the quantitative differences between the predicted and measured values of λ and f as tabulated in Tables 1 and 2.

A recent literature search on the subject of vortex shedding revealed little information regarding the effects of the finite length of the cylinder in the low Reynolds number flow region. At high Reynolds numbers ($R > 1000$), a shorter cylinder results in larger vortex spacing [28]. No information is found at all regarding nonuniform temperature and heat transfer effects on vortex shedding. A detailed analysis of these problems would be very interesting but this is beyond the scope of the present study.

---

*The ratio of the diameter of the electron beam to the width of the welding in the M551 experiments is approximately 0.5.

SECTION III. SPIKING PHENOMENON

One of the undesirable features of an electron beam weld is the so-called "spiking" phenomenon which is a kind of ripple formation in the weld seam during solidification. In the M551 Metals Melting experiments, spiking phenomena were also observed in the partial penetration welds of the stainless steel and tantalum samples (see Figures 1 and 3). Weld ripples were also clearly seen in Figure 5 which is a photograph of the 2219 aluminum specimen after ground tests. Another prominent phenomenon observable in Figure 5 is the apparent disappearance of ripples in the weld region behind the molybdenum film. The molybdenum film has a dimension of 0.5 x 0.5 x 0.0005 inch. It was placed on each of the M551 samples in the weld path at a location of 240 degrees. The purpose of placing a molybdenum film at each sample was to analyze fluid motion during melting by micro-sectioning of the weld.

This section contains a brief discussion and several simple calculations to elucidate the mechanisms of the spiking phenomenon and to suggest possible reasons for the occurrence and disappearance of such a phenomenon.

In an attempt to understand how some electron beam weld defects, such as spikes, cold shuts and base porosity, were formed, Tong and Giedt [29] have performed X-ray analysis of workpieces during actual eb welding process. The results not only verified that electron beam forms a cavity, but also that the cavity oscillates in size and shape. Based on this experimental evidence, the authors of Reference [29] proposed a dynamic model for the formation of the cavity and explained how this model could account for the formation of the aforementioned defects.

It was discovered that the characteristic shapes of an electron beam cavity bear an amazing similarity to the cavities associated with the entry of projectiles into water. When the electron beam strikes the surface of the molten pool, the intense heating causes the material to vaporize and the vapor pressure exerts a downward force on the melt. The vaporization material creates a hypothetical body which behaves like a projectile and penetrates the molten metal. This "projectile" continues to penetrate until the hydrostatic forces cause a deep closure or necking of the cavity. This interrupts the electron beam and separates the original cavity into two cavities, a surface cavity and a subsurface cavity. The lower cavity then ceases to penetrate since the driving force (vapor pressure) is removed and this cavity fills with fluid. The inertia of the deep closure causes an upward flow of fluid until it is overcome by surface vapor pressure and the hypothetical body forms and penetrates again.

An example of the proposed cavity oscillation sequence for 1100 aluminum is shown in Figure 8, which was based on X-ray and radiograph observations of melt cavity.

The above model for the oscillation of the cavity can adequately describe how some of the welding defects are formed. A spike is formed each time the electron beam penetrates to the base of the weld and the severity of the spiking depends on the frequency of the oscillation and the welding speed as well as the material being welded.

When the molten metal flows into the cavity, it can easily trap bubbles of contaminant gases at the base of the weld and, if the cooling rate is sufficiently rapid, the fluid may freeze before the gases can be convected to the surface, thus giving rise to porosity in the fusion zone. Similarly, if the cooling rate is sufficiently rapid, then the melt, as it falls into the cavity, may interrupt the beam long enough for the walls of the spike to freeze so that the fluid, upon falling into the spike, might not bond, thus forming a cold shut or crack. The alternate penetration and closing of the cavity are also very efficient in mixing the melt and results in a very homogeneous fusion zone.

Based on the above dynamic model, Tong and Giedt [29] derived an analytical equation which predicts the spiking frequency. This equation is (see also References [21] and [22])

$$\omega = \frac{\frac{1}{4}\sqrt{\frac{g}{h}}}{\sqrt{\frac{P_v - \frac{2\sigma}{a}}{\rho g h}} - \sqrt{\frac{P_v - \frac{2\sigma}{a} - \rho g h}{\rho g h}}} \qquad (3)$$

where

ω = spiking frequency

g = gravitational acceleration

h = maximum depth of penetration

P_v = vapor pressure of the molten metal

ρ = density of the molten metal

a = radius of the hypothetical body (can be taken approximately as the radius of the electron beam focusing)

The preceding analysis considered welding a horizontal plate from above. The configuration utilized for M551 ground test was that of an electron beam impinging on a vertical disk from the side at a nine to

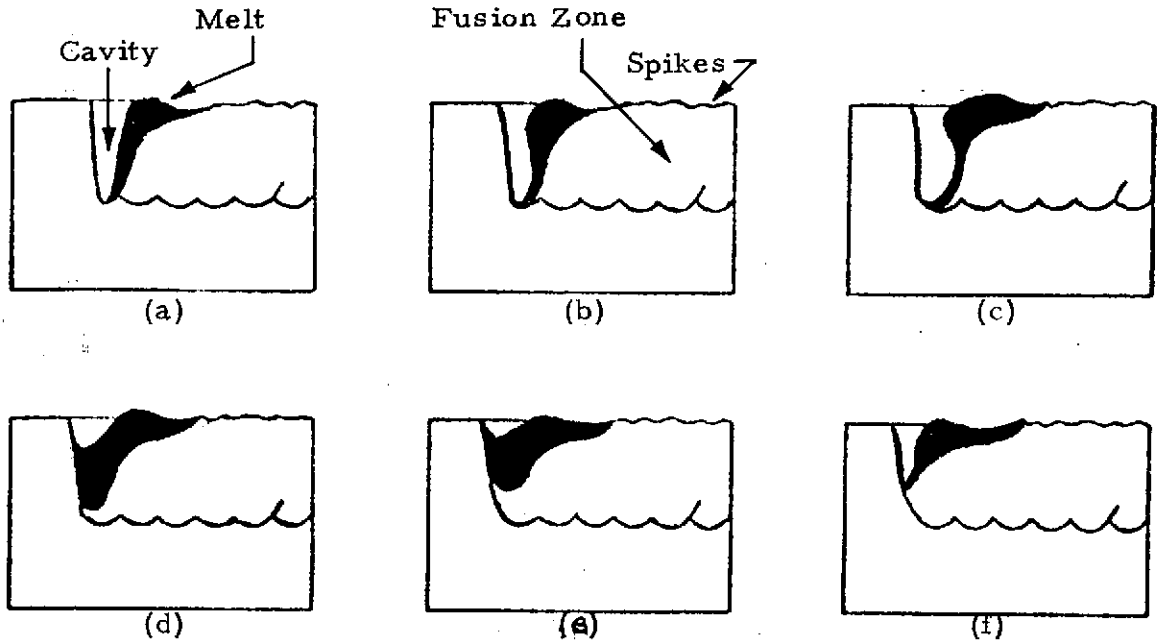

FIGURE 8. CAVITY OSCILLATION SEQUENCE FOR 1100 ALUMINUM [29]

twelve o'clock position with clockwise rotation of the disk past the immobile beam. However, it will be shown below that the effects of g on ω is actually quite small. Equation (3) can also be utilized to predict the trends of spiking formation and the effects of the degree of superheat, surface tension and vapor pressure properties on the severity of the spiking in various materials.

Simple calculations have shown that the spiking frequency is primarily controlled by the magnitude of the vapor pressure and surface tension which are strong functions of temperature or degree of superheat. The effect of g on ω is relatively small because the potential force $\rho g h$ is usually small compared to P_v or $2\sigma/a$.

In a space flight environment, g is of the order $10^{-4} \times g_{earth}$ or smaller, and is essentially negligible in these calculations. In the limit of zero gravity, Eq. (3) becomes

$$\omega = \left(\frac{P_v - \frac{2\sigma}{a}}{4\rho h^2} \right)^{1/2} , \quad g \longrightarrow 0 \qquad (4)$$

It is noted that the higher the vapor pressure and the lower the surface tension, the larger will be the spiking frequency. On the other hand, when the value of $\frac{2\sigma}{a}$ exceeds P_v, there will be no oscillation according to either Eq. (3) or Eq. (4) (the solution becomes imaginary).

The vapor pressure of liquid metals can be calculated from the following equation

$$P_v = e^{B - A/T} \qquad (5)$$

where A and B are empirical constants determined for different materials. The approximate values of A and B for the three M551 materials and molybdenum are tabulated in Table 3.

By using the data in Table 3 and the surface tension data from Reference [25], the values of P_v and $2\sigma/a$ are calculated at different degrees of superheat for the three M551 materials and molybdenum. The results are tabulated in Table 4.

In view of Eq. (4) and the comments following that equation, several observations can be made regarding the calculated data in Table 4.

- At 100% superheat, spikes will form for all the M551 materials.

Table 3

APPROXIMATE VALUES OF A AND B FOR THE M551 MATERIALS

M551 Materials	A (^{o}K)	B
321 Stainless Steel	4.21×10^4	20.05
2219 Aluminum	3.16×10^4	20.2
Tantalum	8.0×10^4	18.9
Molybdenum	6.9×10^4	20.43

Table 4

CALCULATED RESULTS OF P_v AND $2\sigma/a$ FOR THE M551 MATERIALS

Materials	Melting Temp. T_m (^oK)	No Superheat $T = T_m$		20% Superheat $T = 1.2\ T_m$		50% Superheat $T = 1.5\ T_m$		100% Superheat $T = 2.0\ T_m$		At Mo's Melting Temperature $T = 2880^oK$	
		P_v	$2\sigma/a$	P_v	$2\sigma/a$	P_v	$2\sigma/a$	P_v	$2\sigma/a$	P_v	$2\sigma/a$
2219 Aluminum	916	8×10^{-4}	1.97×10^4	0.24	1.80×10^4	81	1.54×10^4	2.59×10^4	1.11×10^4	1.46×10^7	0.16×10^4
321 Stainless Steel	1700	12.1	4.67×10^4	752	4.22×10^4	4.61×10^4	3.56×10^4	2.79×10^6	2.48×10^4	1.20×10^5	3.12×10^4
Tantalum	3270	0.67	5.74×10^4	297	5.03×10^4	1.74×10^4	4.47×10^4	1.06×10^6	3.62×10^4	0.20	6.00×10^4
Molybdenum	2280	40	6.00×10^4	2048	5.53×10^4	1.20×10^5	4.84×10^4	6.10×10^6	3.70×10^4	40.0	6.00×10^4

NOTES: P_v = Vapor pressure in dynes/cm^2

σ = Surface tension in dyne/cm

a $\cong$ Radius of the electron beam

= 0.075 cm

- At 50% superheat, spikes will form in the stainless steel sample.

- No ripples would form in molybdenum if it were welded at 2880°K. (This temperature is greater than 50% superheat for stainless steel and 200% superheat for aluminum.)

- At a given temperature, the vapor pressure of molybdenum is much less than that of stainless steel or aluminum.

- At a given temperature, the surface tension of molybdenum is greater than that of stainless steel or aluminum.

The above observations lead to a possible explanation as to why ripples disappear in the weld zone behind the molybdenum as clearly indicated in Figure 5. The above reasoning is based on the assumption that when the electron beam passes through the molybdenum film, the vapor pressure and surface tension of the melt are controlled by molybdenum instead of the parent material. The validity of this assumption requires, however, further study.

The effect of gravitational acceleration on spiking frequency is shown in Table 5 for the stainless steel sample at three different temperatures. It is seen that g has very little effect on the spiking frequency.

Table 5

CALCULATED SPIKING FREQUENCY FOR STAINLESS STEEL

g (cm/sec^2)	T = 2550°K (50% Superheat)	T = 2883°K (70% Superheat)	T = 3400°K (100% Superheat)
0	28.9*	84.0	468
980	26.2	82.0	467

*Units in cycles per second.

SECTION IV. SUMMARY

Analyses of both the space flight and ground-based tests of the M551 Metals Melting experiments indicate the following:

- Good qualitative agreement was obtained between the measured results of beading frequency and spacing and the predicted values based on the Kármán vortex theory. This tends to support the hypothesis as advanced in Reference [20] that the beading phenomenon which occurred in the stainless steel and tantalum samples was a Kármán vortex street formation.

- Surface tension and sidewall effects appear to be responsible for the absence of beadings in the 2219 aluminum sample after electron beam impingement.

- The dynamic model of cavity oscillation as proposed in Reference [29] can adequately explain the spiking phenomenon observed in the partial welds of the stainless steel and tantalum specimens.

- Calculated results of spiking frequencies for the three M551 samples indicate that the intensity of spiking is primarily determined by the vapor pressure and surface tension properties, and only slightly affected by the level of gravitational acceleration.

- The disappearance of the spiking phenomenon in the weld zone behind the molybdenum film could be caused by the changing of vapor pressure and surface tension of the melt due to molybdenum contamination.

REFERENCES

1. Grodzka, P. G., "Zero-Gravity Solidification," LMSC-HREC D148619-A, March 1970.

2. Fan, C., and P. G. Grodzka, "Mass Diffusion of Gallium Arsenide in a Gallium Solution," LMSC-HREC D225149, June 1971.

3. Grodzka, P. G., and C. Fan, "Natural Convection in Space Manufacturing Processes," Interim Report, LMSC-HREC D162926, July 1971.

4. Grodzka, P. G., C. Fan and R. O. Hedden, "The Apollo 14 Heat Flow and Convection Demonstration Experiments – Final Results of Data Analyses," LMSC-HREC D225333, September 1971.

5. Spradley, L. W., and C. Fan, "A Study of Natural Convection in Low Gravity Solution Growth of Rochelle Salt Crystals," LMSC-HREC D225365, October 1971.

6. Brashears, M. R., "Preliminary Work Plan for Analysis of Materials Processing in Space M512," LMSC-HREC TN D306024, June 1972.

7. Bourgeois, S. V., "Physical Forces and Solidification Theory for Skylab Experiments M551, M552, M553 and M554," LMSC-HREC TN D225975, June 1972.

8. Bourgeois, S. V., "Recommendations for KC-135 Aircraft Testing (M553)," LMSC-HREC TN D225983, June 1972.

9. Bourgeois, S. V., and P. G. Grodzka, "Report on Phase A Progress for Skylab Experiments M551, M552, M553 and M554," LMSC-HREC TN D306014, June 1972.

10. Bourgeois, S. V., "Environmental Conditions and Physical Properties for Skylab Experiments M551, M552, M553 and M554," LMSC-HREC TN D306001, July 1972.

11. Brashears, M. R., "Materials Processing in Space (M512) – Phase A Report," LMSC-HREC D306063, July 1972.

12. Bourgeois, S. V., and P. G. Grodzka, "Convection in Space Processing (M512) – Phase A Report," LMSC-HREC D306065, July 1972.

13. Bourgeois, S. V., "Analysis of Parameters for Molten Braze Alloy Flow in the Skylab M552 Experiment," LMSC-HREC TN D306111, 25 August 1972.

14. Fan, C., "Convection Phenomena in Electrophoresis Separation," LMSC-HREC TR D306300, December 1972.

15. Spradley, L. W., S. V. Bourgeois, C. Fan and P. G. Grodzka, "A Numerical Solution for Thermoacoustic Convection of Fluids in Low Gravity," LMSC-HREC D306140, January 1973.

16. Grodzka, P. G., "Types of Natural Convection in Space Manufacturing Processes: Summary Report," LMSC-HREC TR D306350, January 1973.

17. Grodzka, P. G., and S. V. Bourgeois, "Fluid and Particle Dynamic Effects in Low-g Composite Casting," LMSC-HREC TR D306402, February 1973.

18. Brashears, M. R., "Science and Engineering Information for M551 and M553 Experiments," LMSC-HREC TN D306615, April 1973.

19. Brashears, M. R., "Research Study on Materials Processing in Space Experiment M512 – Phase B Report," LMSC-HREC TR D306700, August 1973.

20. Brashears, M. R., and S. J. Robertson, "Research Study on Materials Processing in Space Experiment M512 – Final Report," LMSC-HREC TR D306954, December 1973.

21. Bourgeois, S. V., "Convection Effects on Skylab Experiments M551, M552 and M553 – Phase C Report," LMSC-HREC TR D306955, December 1973.

22. Bourgeois, S. V., and M. R. Brashears, "Fluid Dynamics and Kinematics of Molten Metals in the Low Gravity Environment of Skylab," Paper No. 74-205, presented at the AIAA 12th Aerospace Sciences Meeting, Washington, D. C., 1 February 1974.

23. Bourgeois, S. V., "Physical Forces Influencing Skylab Experiments M551, M552 and M553 – Summary Report," LMSC-HREC TR D390056, January 1974.

24. Roshko, A., "On the Development of Turbulent Wakes from Vortex Streets," NACA TN 2913, 1953.

25. Beer, S. Z. (Ed.), Physics and Chemistry of Liquid Metals, Marcel Dekker, Inc., New York, 1972.

26. Taneda, S., "Experimental Investigation of Vortex Streets," J. Phys. Soc. Japan, Vol. 20, 1965, p. 1714.

27. Shair, F.H. et al., "The Effects of Confining Walls on the Stability of the Steady Wake Behind a Circular Cylinder," J. Fluid Mechanics, Vol. 17, 1963, p. 546.

28. Papailiou, D., and P. S. Lykondis, "Turbulent Vortex Street and the Entrainment Mechanism of the Turbulent Wake," J. Fluid Mechanics, Vol. 62, Part 1, 1974, p. 11.

29. Tong, H., and W.H. Giedt, "A Dynamic Interpretation of Electron Beam Welding," Welding J., June 1970, p. 259s.